Effect of γ-radiation on structural, morphological, magnetic and dielectric properties of Zn–Cr substituted nickel ferrite nanoparticles

Published: 01 November 2018

Volume 30, pages 56–68, (2019) Cite this article

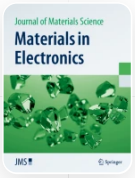

Journal of Materials Science: Materials in Electronics

Aims and scope

Submit manuscript

Vishwanath K. Mande, Jitendra S. Kounsalye, S. K. Vyawahare & K. M. Jadhav

Abstract

In the present work nano-sized zinc and chromium substituted simultaneously in nickel ferrites $Ni_{1-x}Zn_xFe_{2-x}Cr_xO_4$, (Ni–Zn–Cr) nanoparticles with $x = 0.0$, 0.2, 0.4, 0.6, 0.8 and 1.0 were successfully synthesized through a sol–gel auto-combustion technique using citric acid as a fuel. All the prepared samples have been irradiated by γ-rays of ^{60}Co source with 7 Mrad at a dose rate of 0.1 Mrad/h to investigate the irradiation effect on the structural, morphological, magnetic and dielectric properties of all the prepared samples. Ni–Zn–Cr nanoparticles were investigated by X-ray diffraction (XRD), Fourier transform infrared spectroscopy (FT-IR), field emission scanning electron microscopy (FE-

SEM) to study their structural and morphological changes. The magnetic properties were studied by vibrating sample magnetometer (VSM) at room temperature before and after irradiation. XRD patterns confirm the formation of pure mono-phase of a cubic spinel structure for all the prepared samples. The two prominent absorption bands in FT-IR spectra also confirm the formation of the spinel structure. The FE-SEM image of un-irradiated samples show agglomerated and almost spherical shape particles morphology; while γ-irradiated samples show some scratched morphology. Dielectric constant and dielectric loss tangent decreases with an increasing zinc and chromium concentration of the unirradiated and after γ-irradiated. Overall; the structural, morphological, magnetic and dielectric properties of the present samples were significantly altered after γ-irradiation. Therefore, low dielectric constant and dielectric loss tangent is attractive due to its potential in device applications.

1 Introduction

Ferrites are very excellent attractive materials and are a group of technological most important magnetic materials that are used in the manufacturing of magnetic, electronic devices, etc [1]. Ferrites have excellent dielectric properties apart from their good electrical and magnetic properties [2]. These are valuable in designing a good microwave device such as Isolators, circulators etc [3].The spinel ferrite is one of the most important candidates of attractive ceramic materials due to their remarkable applications [4]. The spinel ferrite has face-centered cubic (FCC) structure in which oxygen atoms are

cubic close packed in which the magnetic ions are distributed among two dissimilar lattice sites tetrahedral (A) and octahedral [B] sites [5, 6]. The magnetic and electrical properties of ferrites are dependent on the relative cation distribution on the different sites [7]. The cation distributions depend on the chemical composition, sintering conditions and the method of preparation [8]. The simultaneous substitution of nonmagnetic zinc ion and magnetic chromium ion in nickel ferrite leads to the modification of structural, morphological and magnetic properties [6, 9]. Pure nickel ferrite and substituted nickel ferrites are the most important candidate of spinel ferrite [10, 11]. According to the reported data, the crystal structure of nickel ferrite is an inverse spinel ferrite and possesses high electrical resistivity and low eddy current losses [12, 13]. The substitution of zinc and chromium in nickel ferrite modifies the properties of nickel ferrite which are valuable in various device applications [14]. Ni–Zn–Cr is very excellent magnetic material because of their high electrical resistivity, high saturation magnetization and high magnetic permeability, low power loss and superparamagnetism depend on the particle size of the material [15, 16].

Several synthesis methods have been used to prepare nano particles such as sol–gel auto-combustion method [17,18,19], co-precipitation [20], hydrothermal method [21, 22], high energy ball milling [23], oxalate decomposition route [24], micro-emulsion [25], etc. Among the wet chemical methods, the sol–gel auto combustion method has several significant advantages due to its simplicity including proper stoichiometric, low cost, uniform size distribution and also compositional homogeneity. These methods have been adopted to prepare zinc and chromium simultaneously substituted in nickel ferrite nanoparticles using citric acid as a fuel. Nowadays, radiation techniques are used for processing and studying superior materials in the manufacturing facilities and therapeutic instruments, such as generating facilities, nuclear fusion reactors, magnetic resonance imaging scanner and computerized tomography, space craft and satellite [26, 27]. The material scientist is doing many experiments to study the effect of different irradiation such as swift heavy ions, laser; gamma ray on the properties of ferrite materials depends on the potential applications [28,29,30]. Gamma irradiation is a powerful tool to enhance crystallographic defects to modify the structural, electrical and magnetic properties of ferrite materials with compositions. Recently, many researchers and scientists were synthesized the different systems; $Co_{0.6}Zn_{0.4}Mn_xFe_{2-x}O_4$ Hamada et al. [31], $Li_{0.5}Fe_{2.5}O_4$ ferrite Mane et al. [32], $Mn_{0.5}Zn_{0.5}Fe_2O_4$ nanoferrite Angadi et al. [33] and also on $Ni_{1-x}Zn_xFe_2O_4$ spinel ferrites Karim et al. [34] and studied the effects of gamma irradiation on the structural, electrical, and magnetic properties. The effect of gamma irradiation of very low dosage on Mn–Zn spinel ferrites was also reported [35]. However, to our knowledge, very few reports are available in the literature on the effect of gamma irradiation on the properties of Ni–Zn–Cr spinel ferrite synthesized by sol–gel auto combustion method.

In the present work, we have studied systematically the effect of co-substitution of zinc and chromium

ion in nickel ferrite on the structural, morphological and magnetic properties using standard cost effective sol–gel auto combustion methods. The properties were investigated before and after irradiation to understand the effect of gamma irradiation and the results are presented.

2 Experimental methods and materials

A nickel nanoferrite system with simultaneous substitutions of zinc and chromium with the general chemical formula $Ni_{1-x}Zn_xFe_{2-x}Cr_xO_4$ nanoparticles (x = 0.0, 0.2, 0.4, 0.6, 0.8 and 1.0) have been synthesized using the sol–gel auto-combustion method. Analytical Reagent grade nickel nitrate [$Ni(NO_3)_2.6H_2O$], zinc nitrate [$Zn(NO_3)_2.6H_2O$], iron nitrate [$Fe(NO_3)_3.9H_2O$], chromium nitrate [$Cr(NO_3)_3.9H_2O$], and citric acid ($C_6H_8O_7$), and ammonia were used as a starting materials. All the chemicals such as nitrates of 99.9% purity were purchased from MERCK. In our earlier publication, the details of the synthesis procedure were reported [36]. The as-synthesized nanopowders were then sintered at 600 °C for 5 h in the air surroundings to eliminate the whole impurities. The sintered nanopowder has been yet again ground and pelletized. These pellets are finely sintered to 900 °C for 9 h. The prepared nanoparticles were systematically ground in a pestle mortar and after that utilized for further characterizations. Figure 1 shows the schematic flow chart of sol–gel auto-combustion synthesis method of Zn–Cr substituted $Ni_{1-x}Zn_xFe_{2-x}Cr_xO_4$ nanoparticles.

Fig. 1

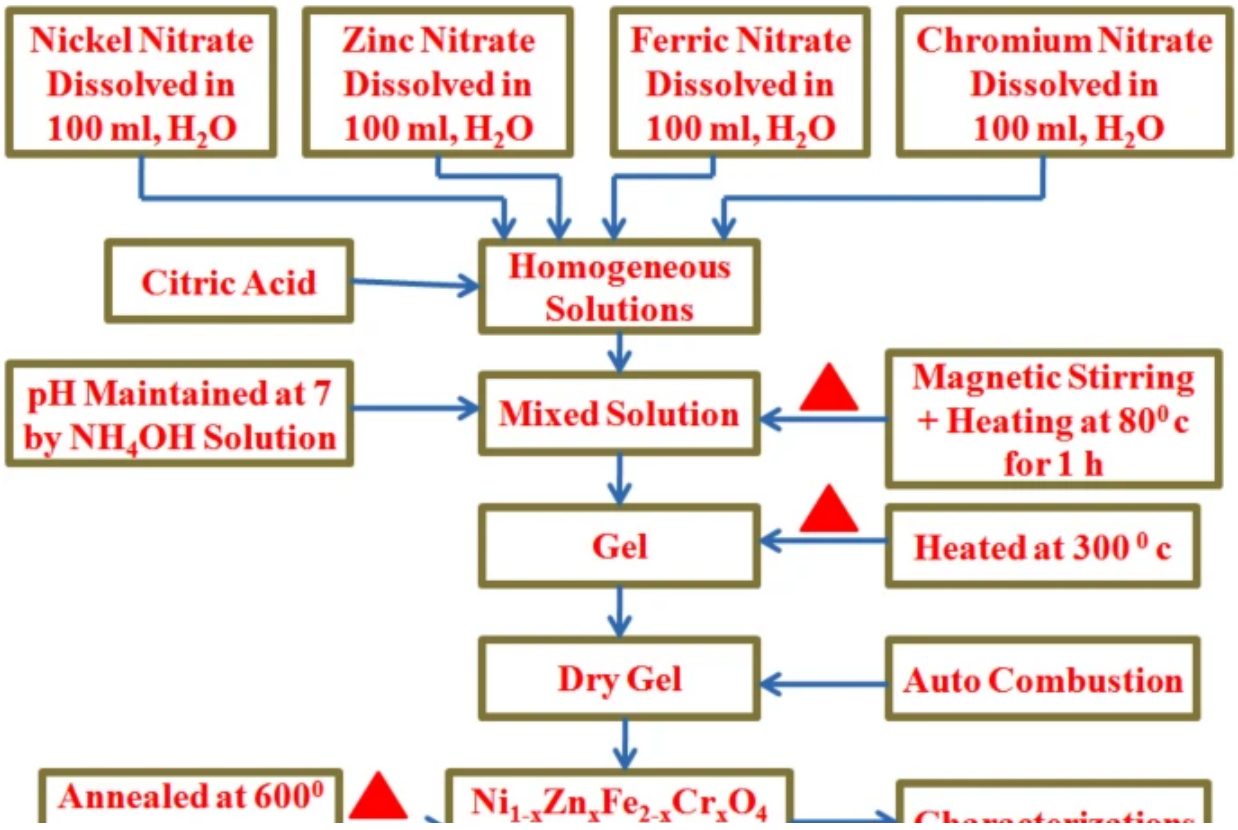

Schematic representation flow chart of sol–gel auto combustion synthesis procedure for $Ni_{1-x}Zn_xFe_{2-x}Cr_xO_4$ $x = 0.0$, 0.2, 0.4, 0.6, 0.8, and 1.0 Nps

All the prepared samples were irradiated by using energetic source ^{60}Co of gamma radiation. The total exposure dose time estimated for irradiation was 5 days, 60 h to complete the total dose of 7 Mrad with a dose rate of 0.1 Mrad/h. The phase formation of all the samples was confirmed by the powder X-ray diffraction (XRD) studies using model PW-1710 by Phillips X-ray diffractometer having Cu-K\(\alpha\) radiation (λ=0.15405 nm), at room temperature in the 2θ scanning range from 20 to 80°, at a speed of scanning ~ 2°/min. Fourier Transform Infrared Spectroscopy (FT-IR) spectra in the range of 400–4000 cm^{-1} were recorded using a perkin- Elmer spectrometer (spectrum 1000). The surface morphology studied of un-irradiated and γ-irradiated of the samples was characterized by field emission scanning electron microscopy (FE-SEM), (Model JOEL-JSM 840). The magnetic properties of un-irradiated and irradiated of the ferrite samples were measured at room temperature by using vibrating sample magnetometer (VSM) (Lakeshore VSM 7410 Model) with the maximum applied field of \(\pm\)15 kOe. The dielectric properties were studied at room temperature using (Hioki model 3532-50) with a digital LCR-Q meter (Japan) and in the frequency range of 50 Hz to 5 MHz before and after γ-irradiated.

3 Results and discussion

3.1 X-ray diffraction (XRD)

The XRD patterns of all the prepared $Ni_{1-x}Zn_xFe_{2-x}Cr_xO_4$ nanoparticles with ($x = 0.0$, 0.2, 0.4, 0.6, 0.8 and 1.0) before and after γ-irradiation are depicted in Fig. 2. XRD patterns show all the allowed Bragg's reflection planes namely (220), (311), (222), (400), (422), (511), (440), (620), (533), related to cubic spinel structure in both the cases. The XRD patterns match well with (JCPDS) card no-74-2081:$NiFe_2O_4$; (JCPDS) card no-73-1963: $ZnFe_2O_4$ and also match well with the standard of the American Society for Testing and Materials (JCPDS) card no-019-0629 for both un-irradiated and irradiated samples. There are no extra significant impurity peaks observed in the XRD patterns. All the prepared samples show XRD planes with depict sharp peaks signifying nanocrystalline nature. Using the XRD data different structural parameters were calculated by standard relations. The lattice parameters of the present system are calculated by using 2θ values of Bragg's reflection planes and the values are displayed in Table 1. The lattice parameters for nickel ferrite ($x = 0.0$) is in good agreement with our previous work. Table 1 shows that, the lattice parameters increases with zinc–chromium

simultaneous substitution with obeying the Vegard's law [37]. The increase in lattice parameters is attributed to the replacement of ionic radii of (A) and [B] sites. The ionic radius of Zn^{2+} (0.82 Å) is larger than Ni^{2+} (0.78 Å) at (A) site and also Fe^{3+} (0.67 Å) is larger than Cr^{3+} (0.61 Å) ions in [B] site which creates the lattice strain. Thus, the lattice parameter to be increased in the present work, a similar trend of lattice parameters was reported by literature S. Karimi et al. [6]. Further; on irradiation it is obvious from Fig. 2 that the peak positions are shifted to higher 2θ values and also the peak intensities are decreased. The widths of the peaks are enhanced than that of the un-irradiated samples. Also, it can be seen from Table 1 that the value of lattice parameters decreases after irradiation, because of the lattice vacancies generated after irradiation causes distortion and deviation from the spinel cubic structure. This may be due to the gamma irradiation formed the compressive strain and furthermore generated some disorder in the lattice structure. A similar result was observed in gamma irradiated $Ni_{1-x}Zn_xFe_2O_4$ samples [34].The crystallite size (t) of all the prepared samples has been calculated by using the Debye–Scherrer's formula [38]. The value of crystallite size for all the samples unirradiated and after γ-irradiated is presented in Table 1.The high intense peak (311) was selected for the calculation of crystallite size. From Table 1, it is clear that the value of crystallite size (t) is found to be decreased after γ-irradiation. The energy rich ions penetrate the sample along the path of the ion beam and lead to a material alteration. In the process; the heavy ions loss their energy which in revolve generates defects and partial amorphization resulting in a decrease in the crystallite size [39]. In another reason, after γ-irradiated could be modify the ratio of Fe^{2+}/Fe^{3+} ions in octahedral [B] site since a result of ($\gamma + Fe^{2+} \rightarrow Fe^{3+} + e^-$) which gets to a change in the crystal structure. Similar type of explanation is reported in the literature [40]. The X-ray density d_x for all the prepared samples were determined from molecular weight, volume of the unit cell and its natures are presented in Fig. 3(a) and (b) respectively, also the values are tabulated in Table 1. The X-ray density is found to be increased with increase in the concentration of Zinc-Chromium simultaneous substitution. From the Table 1, it is observed that the X-ray density increases after γ-irradiation. This is attributed to an increase in mass is more than the increase in lattice parameter.

Fig. 2

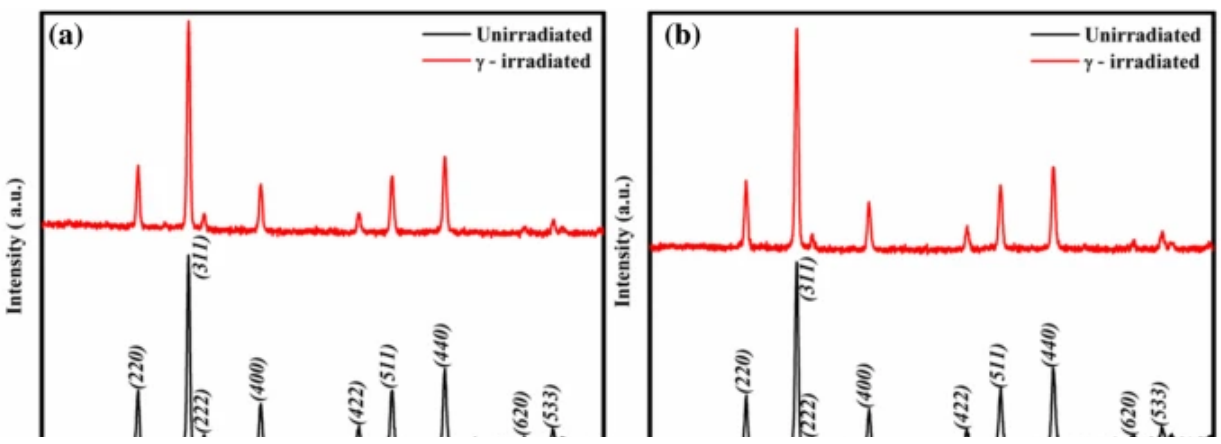

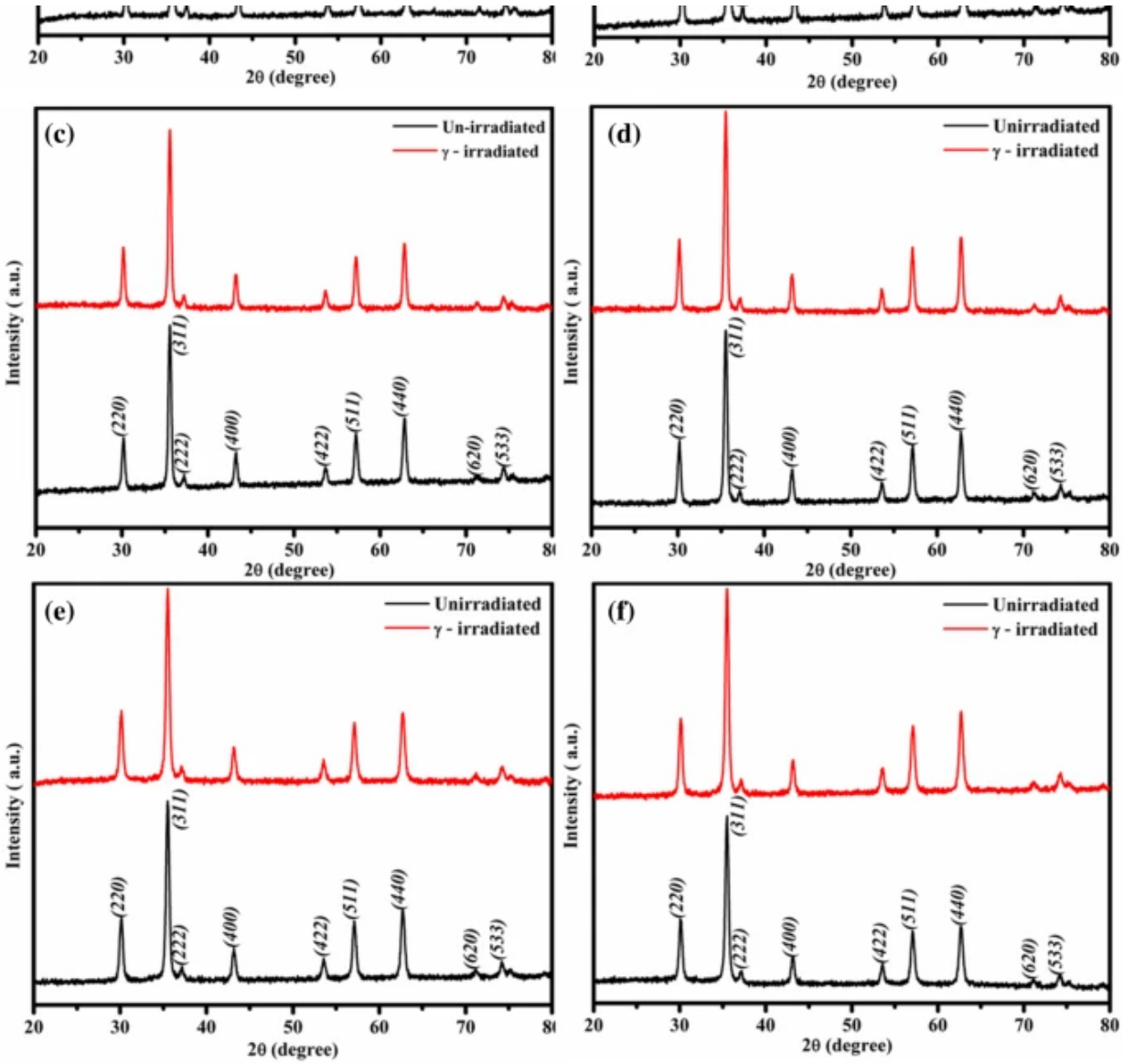

X-ray diffraction patterns of Unirradiated and \(\gamma\)-irradiated $Ni_{1-x}Zn_xFe_{2-x}Cr_xO_4$ NPs for (**a**) $x = 0.0$, (**b**) $x = 0.2$, (**c**) $x = 0.4$, (**d**) $x = 0.6$, (**e**) $x = 0.8$, (**f**) $x = 1.0$

Table 1 Unit cell volume (V), lattice constant (a), X-ray density (d_x), crystallite size (t) for before and after gamma irradiation samples $Ni_{1-x}Zn_xFe_{2-x}Cr_xO_4$ nanoparticles

Fig. 3

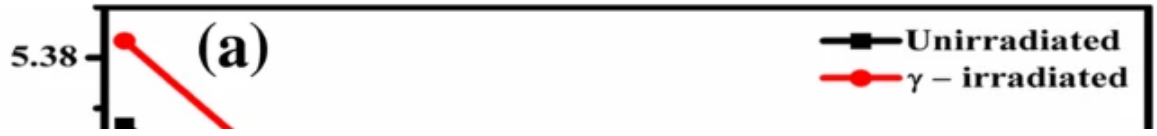

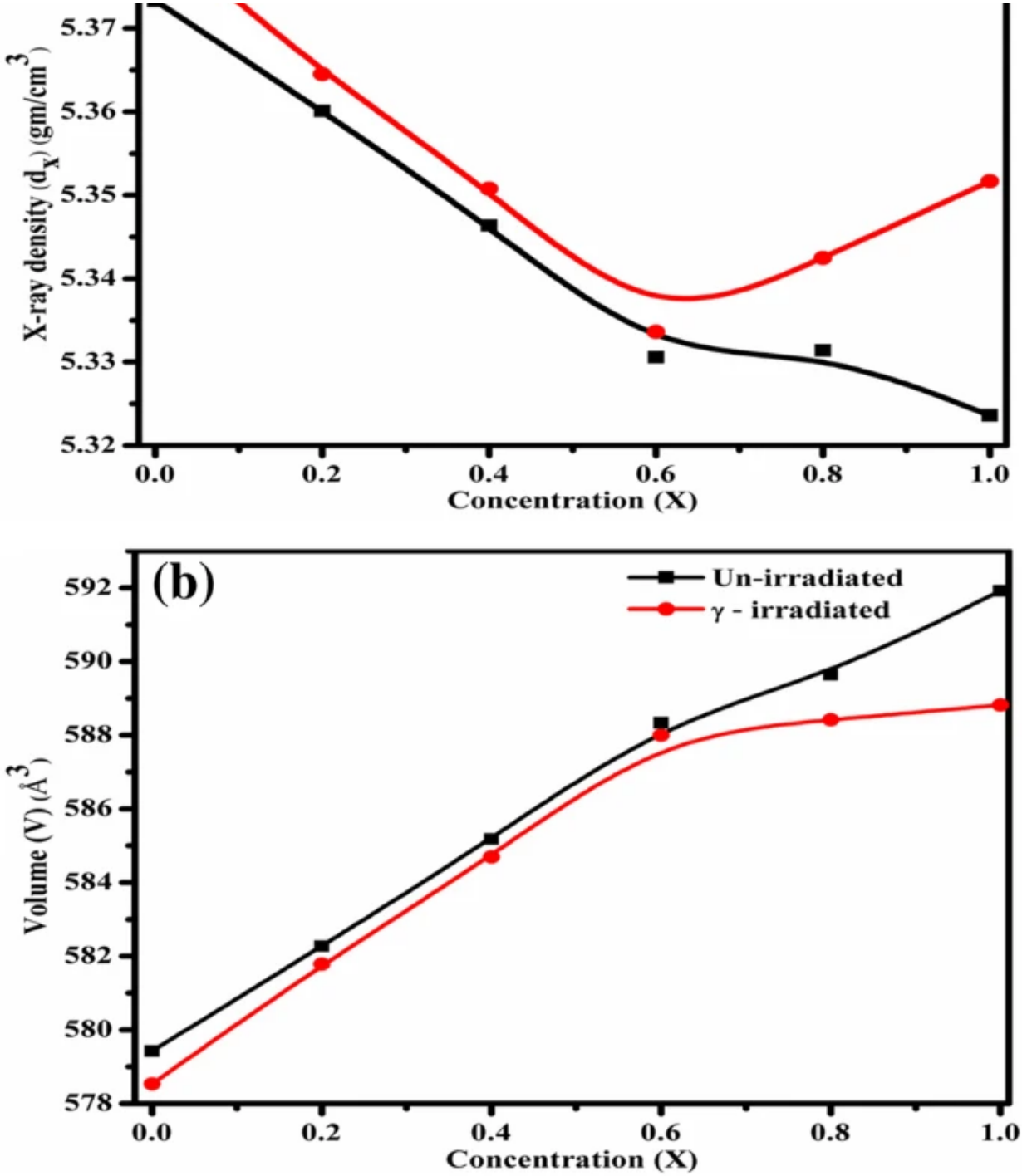

(**a**) Variation of X-ray density (d_x) with Zn, Cr composition (x). (**b**) Variation of Volume (V) with Zn, Cr composition (x) for $Ni_{1-x}Zn_xFe_{2-x}Cr_xO_4$ NPs

The another structural parameters, such as the values of the tetrahedral bond length (d_{AX}), octahedral bond length (d_{BX}), tetrahedral edge (d_{AXE}), shared and unshared octahedral edge (d_{BXE}) and (d_{BXEU}), the tetrahedral (A) site ionic radii (r_A) and the octahedral [B] site ionic radii (r_B) were determined for all the samples by using the standard relation listed as following Eqs. (1–5) [41].

$${d_{AX}}=~a\sqrt {3~} \left({u - \frac{1}{4}} \right)~$$

(1)

$${d_{BX}}=a\sqrt {\left({3{u^2}} \right) - \left({\frac{{11}}{4}} \right)u+\left({\frac{{43}}{{64}}} \right)} ~$$

(2)

$${d_{AXE}}=~a\sqrt {2~} \left({2u - \frac{1}{2}} \right)$$

(3)

$${d_{BXE}}=~a\sqrt {2~} \left({1 - 2u} \right)~$$

(4)

$${d_{BXU}}=a\sqrt {(4{u^2}) - (3u)+\left({\frac{{11}}{{16}}} \right)} ~$$

(5)

where 'a' is the lattice parameter and 'u' is the oxygen positional parameter, for these ideal value of 'u' (0.381 nm) for the precisely cubic closed-packed spinel structure. All of these structural parameters are presented in Tables 2 and 3. The values of all the structural parameters are decreasing with increase in Zinc–Chromium simultaneous substitution for both unirradiated an after γ-irradiated. All these parameters depend on the lattice parameter.

Table 2 Tetrahedral bond (d_{AX}) and octahedral bond (d_{BX}), tetra edge (d_{AXE}) and octa edge (d_{BXE}) (shared and Unshared), the tetrahedral A-site ionic radii (r_A) and the octahedral B-site ionic radii (r_B) for before and after gamma irradiation samples $Ni_{1-x}Zn_xFe_{2-x}Cr_xO_4$ nanoparticles

Table 3 Tetrahedral A-site ionic radii (r_A) and the octahedral B-site ionic radii (r_B), Infrared absorption frequency band position (v_1 and v_2) for before and after gamma irradiation samples $Ni_{1-x}Zn_xFe_{2-x}Cr_xO_4$ nanoparticles

3.2 FT-IR studies

Fourier transform infrared spectroscopy (FT-IR) spectra of the un-irradiated and γ-irradiated samples are depicted in Fig. 4(a) and (b). The FT-IR spectra was recorded in the wave number range of 4000–400 cm^{-1} at room temperature. In the ferrites, the crystal structure are mutually bounded with the nearest neighbors by corresponding forces (ionic, covalent or vander Waals) [42].

Fig. 4

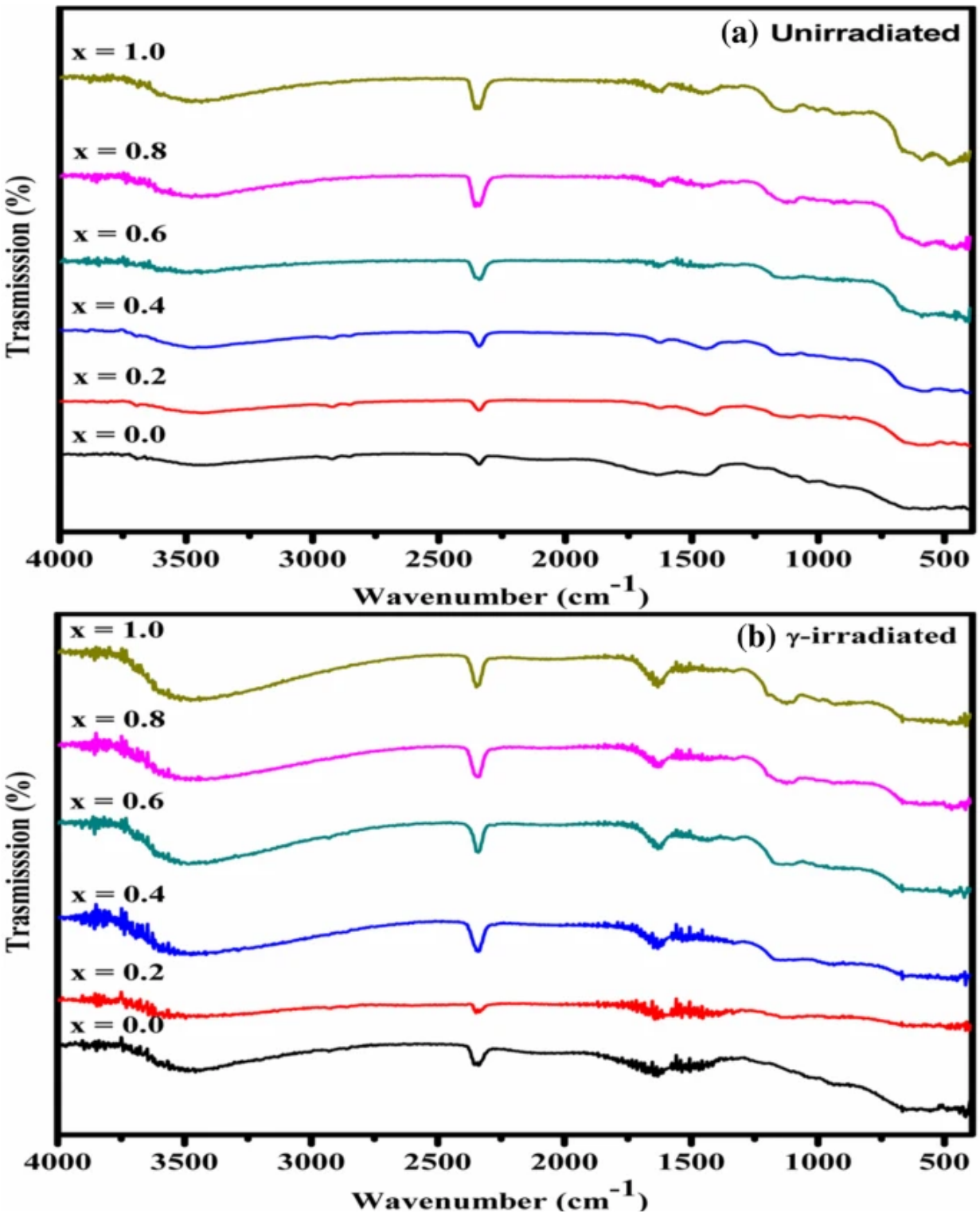

(**a**) FT-IR spectra of Unirradiated and (**b**) γ-irradiated for $Ni_{1-x}Zn_xFe_{2-x}Cr_xO_4$ (x = 0.0, 0.2, 0.4, 0.6, 0.8, 1.0) NPs

According to Waldron law, the geometrical configuration of the oxygen, the metal ions occupy two different sublattices namely tetrahedral (A) site and octahedral [B] site. These bands are the common features of all the spinel structure of ferrite. In the present study, FT-IR spectra show the two prominent absorption bands (υ_1, υ_2) observed at 567–694 cm^{-1}, 430–486 cm^{-1} and 611 cm^{-1}, 420–480 cm^{-1} for unirradiated and after γ-irradiated which are summarized in the Table 3. The high frequency peak (υ_1) lies in the range of 587 cm^{-1}corresponding to the intrinsic stretching vibrations of tetrahedral metal–oxygen complexes, while low frequency peak (υ_2) band observed in the range 430 $cm^{-1}$is attributed to the vibrations of octahedral metal–oxygen complexes. Similar kinds of results are observed in the literature [43].

The FT-IR spectra confirmed the formation of single phase cubic spinel structure. Our results well agree with the reported data. Also, the remaining groups of combustion process can be observed that absorption peaks with wave number at 3502 cm^{-1}, 2343 cm^{-1}, 1448 cm^{-1}, 1627 cm^{-1}, 1120 $cm^{-1}$are attributable to characteristic peaks of a hydroxyl group (symmetric and asymmetric) and a carboxyl group NO_3, ions respectively [44, 45]. It indicates significant energy produced during the combustion process is not highly adequate to create these groups, which is not taking part in the reaction during the combustion.This may be due to modification in the inter-nuclear distance of Fe^{3+}–O^{2-} on the correspondent lattice sites. These results are defects or migration of a few ions into interstitial positions as effect to after γ-irradiated.

3.3 Surface morphology studies

The typical surface morphological properties of the Ni–Zn–Cr ferrite samples were investigated by using field emission scanning electron microscopy (FE-SEM). The representative FE-SEM micrographs of samples with composition x = 0.0, and 0.4 unirradiated and after γ-irradiated are shown in Fig. 5(a–d). From the Fig. 5(a–d) it is clear that some particles are agglomerated and produced big clusters. The grain growth of nanoparticles is attributed to the migration of pores in the solid solution to the grain boundaries. It can be observed that the grain size increases with increase in zinc and chromium concentration than as shown in XRD data. The average grain sizes of the prepared samples were calculated from the linear intercept method [46], and are listed in Table 4. Figure 5(b–d) is evidently shown that after γ-irradiation, it has been a strong influence on the surface morphology of the samples that the defects are created in the material. Micrographs showed changes in the grain size

and grain boundaries. There is some change in the grain size and amorphization at the grain boundaries due to after γ-irradiated.

Fig. 5

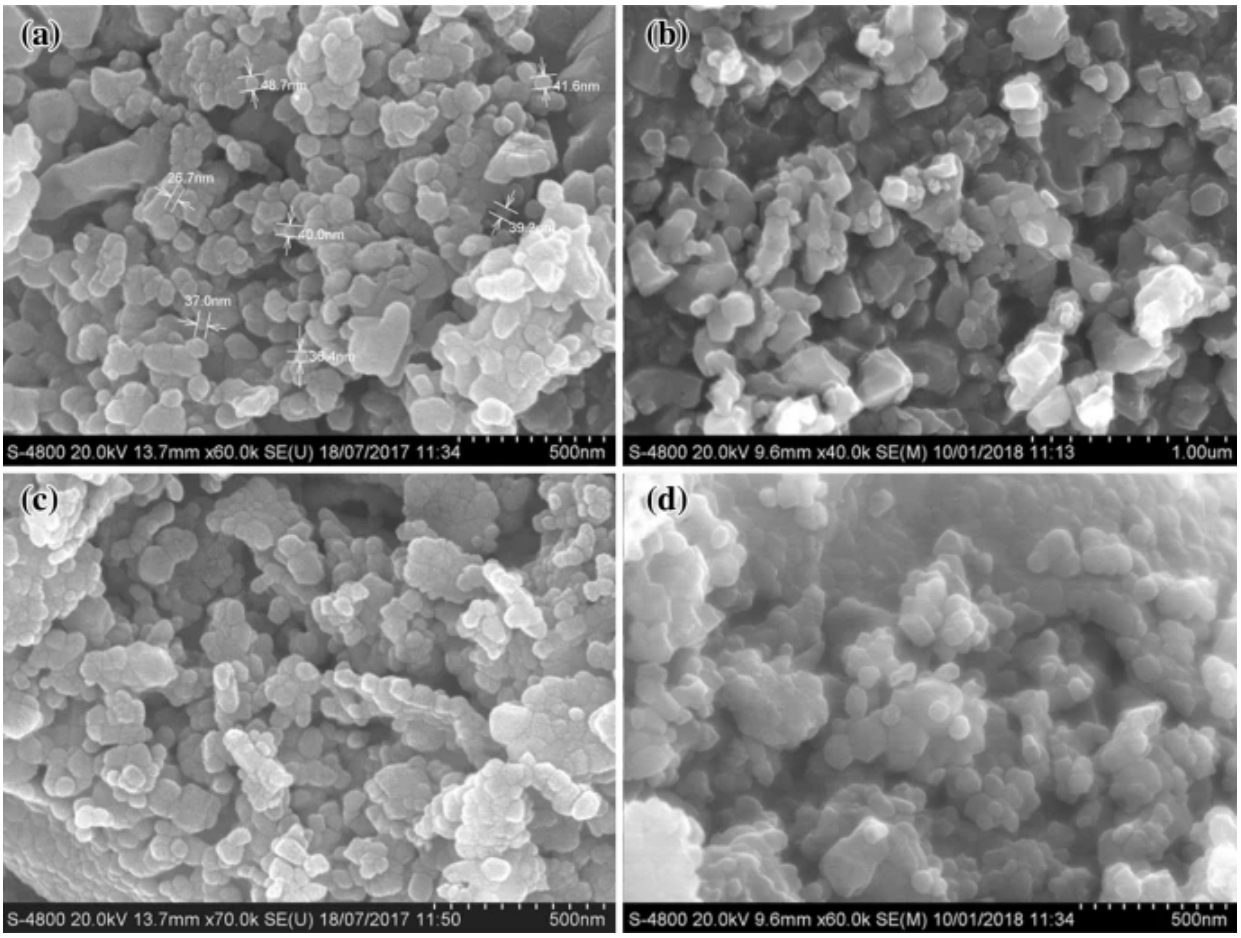

(**a**–**d**) FE-SEM micrographs of typical samples (**a**) $x = 0.0$, (**c**) $x = 0.4$ unirradiated and (**b**) $x = 0.0$, (**d**) $x = 0.4$; \(\gamma\)-irradiated for $Ni_{1-x}Zn_xFe_{2-x}Cr_xO_4$ NPs

Table 4 Grain size (G) and elemental percentage (At %) from EDS graph of $Ni_{1-x}Zn_xFe_{2-x}Cr_xO_4$ nanoparticles

The elemental compositions of the typical samples were calculated by EDS spectrum of $Ni_{1-x}Zn_xFe_{2-x}Cr_xO_4$ samples with ($x = 0.0$ and 0.4) nanoparticles are presented in Fig. 6(a–d). By the observation of EDS spectrum analysis confirmed the presence of all the elements such as, Ni^{2+}, Zn^{2+},

Fe^{3+}, Cr^{3+}, O^{2-} ions in the synthesized samples. The EDS results confirm that there is no traces of impurity elements were found in the present system. The calculated atomic and weight percentage of the synthesized samples are consistent with the composition from EDS analysis and obtained values are listed in Table 3.

Fig. 6

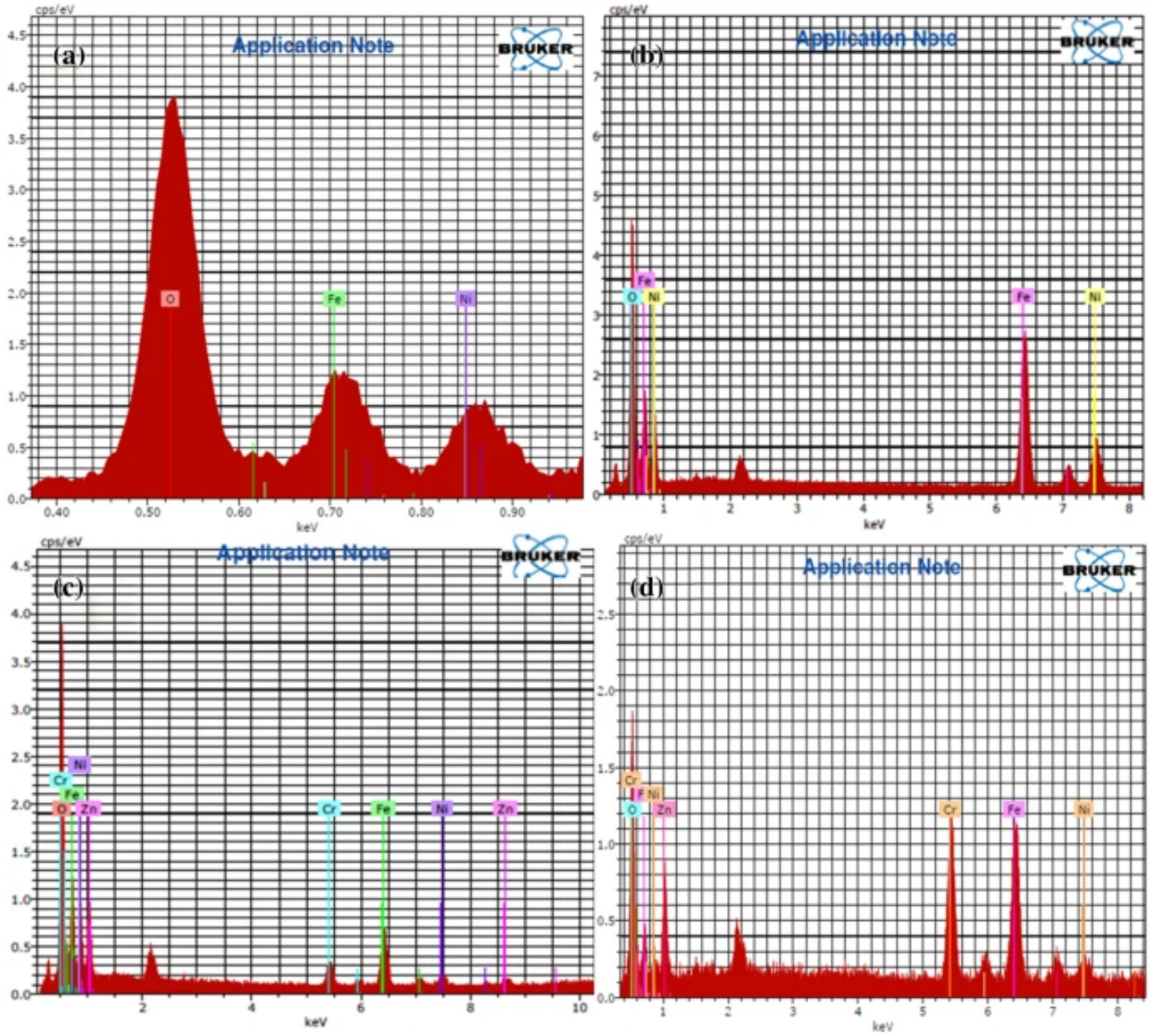

(**a**–**d**) EDS spectra of typical samples (**a**) $x = 0.0$; (**c**) $x = 0.4$ unirradiated and (**b**) $x = 0.0$; (**d**) $x = 0.4$ \(\gamma\)-irradiated for $Ni_{1-x}Zn_xFe_{2-x}Cr_xO_4$ NPs

3.4 Magnetization studies

The magnetic measurement of investigated samples was studied by using a vibrating sample magnetometer (VSM). The room temperature (VSM) investigation was carried out with the maximum

applied magnetic field up to ± 15 kOe and is illustrated in Fig. 7(a) and (b). The M-H loops of shape and width depend on various factors such as chemical composition, crystallite size, porosity, grain size and gamma irradiation, etc. It can be observed that narrow M-H loops reveal the soft nature of the ferrite material. From the M-H loops, the values of saturation magnetization (M_s), a remanent magnetization (M_r), coercivity (H_c), loop squareness ratio (M_r/M_s) and magnetic moment \((~{\eta _{\rm B}})\) unirradiated and after γ-irradiated are summarized in Table 5. From the Table 5, it is observed that the saturation magnetization (M_s) and also coercivity (H_c) decreases with zinc and chromium simultaneously substituted in nickel ferrites. The saturation magnetizations (M_s) behave in random slowly decrease due to an unexpected change in site preference of after γ-irradiation.

Fig. 7

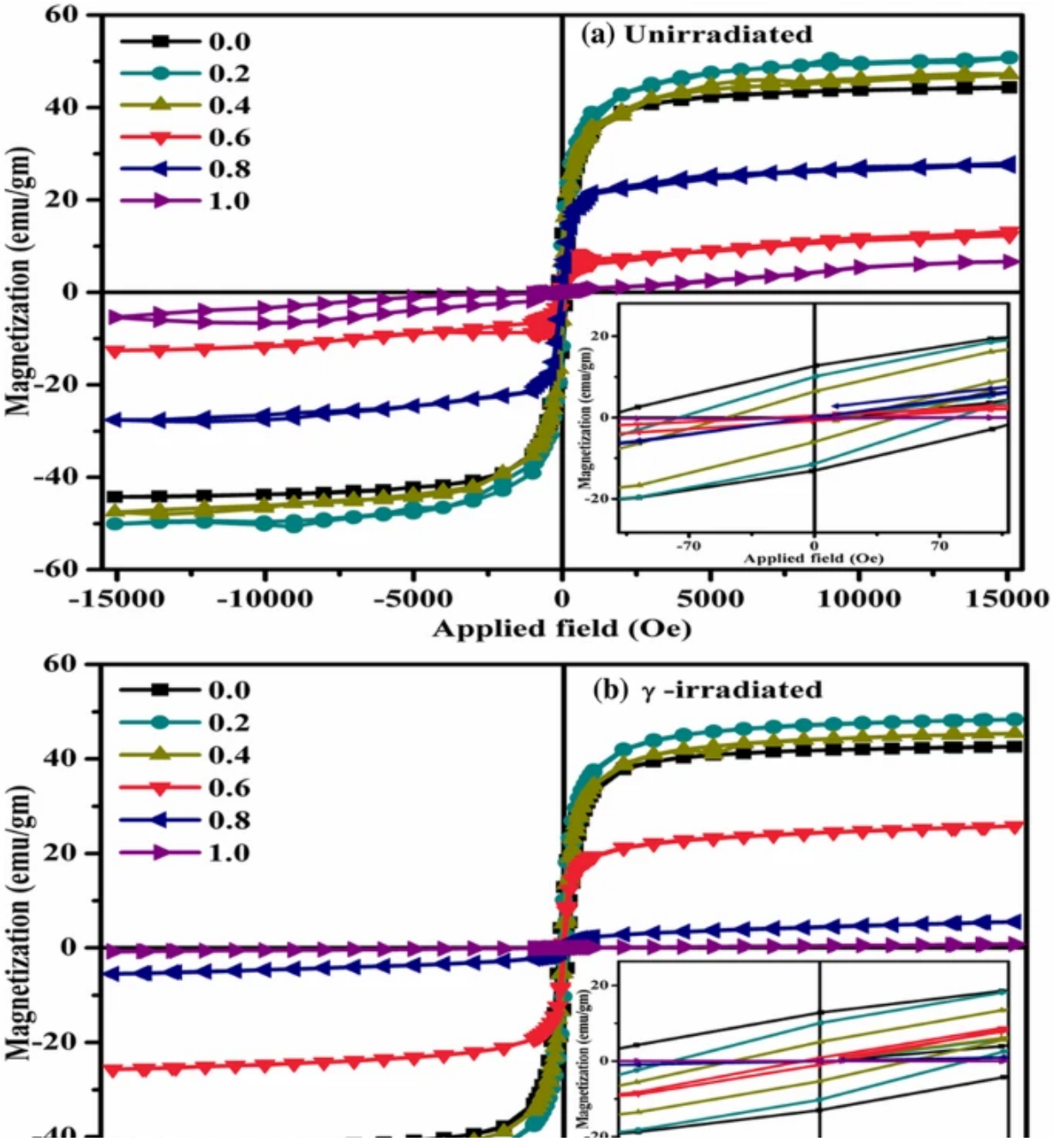

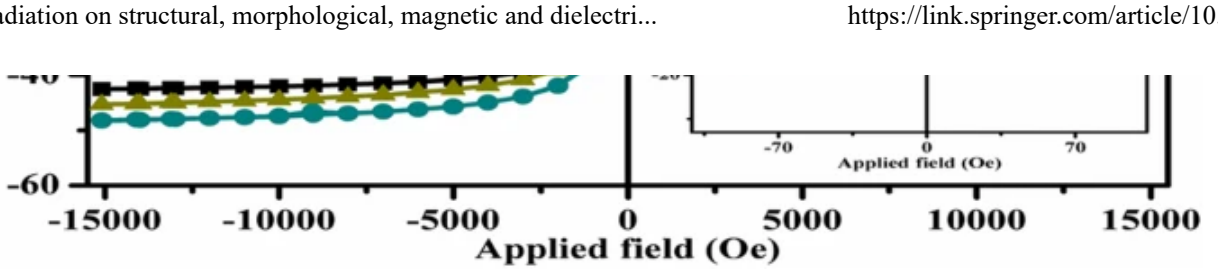

Hysteresis loops for $Ni_{1-x}Zn_xFe_{2-x}Cr_xO_4$ (x = 0.0, 0.2, 0.4, 0.6, 0.8 and 1.0) (**a**) Unirradiated and (**b**)\(~\gamma\)-irradiated of NPs

Table 5 The room temperature of saturation magnetization (M_s), remanent magnetization (M_r), coercivity (H_c) remenance ratio (M_s/M_r), magnetic moment (nB) for before and after gamma irradiation samples $Ni_{1-x}Zn_xFe_{2-x}Cr_xO_4$ nanoparticles

In the present system, $Ni_{1-x}Zn_xFe_{2-x}Cr_xO_4$ nanoparticles with (x = 0.0, 0.2, 0.4, 0.6, 0.8 and 1.0) the values of saturation magnetization observed to decrease with zinc and chromium simultaneously substituted in nickel ferrites both of unirradiated and after γ-irradiated. It is well-known that $NiFe_2O_4$ ferrite has an inverse spinel structure in which the iron cations partially occupy tetrahedral (A) sites and another half occupy octahedral [B] sites. From the M-H loop, it is observed that the saturation magnetization decreases with increasing zinc and chromium ions simultaneous substitution in $NiFe_2O_4$ ferrite and also same behavior observed for gamma irradiation. It may be due to the weakening of (A-B) superexchange interactions between the tetrahedral (A) site and octahedral [B] site. Zn^{2+} ions have a strong tendency to occupy tetrahedral (A) sites and Cr^{3+} ions have a strong tendency to occupy octahedral [B] sites through their substitution in $NiFe_2O_4$ ferrite of before and after gamma irradiation. The decrease in saturation magnetization due to the replacement of the Zn^{2+} ion has tiny magnetic moments (0\({\mu _{\rm B}}\)), in comparison with Ni^{2+} (2\({\mu _{\rm B}}\)), and also Cr^{3+} ion have small magnetic moments (3\({\mu _{\rm B}}\)), in comparison with Fe^{3+} ions (5\({\mu _{\rm B}}\)) which results in decrease of a magnetic moments at [B] site. According to Neel's two sub-lattice model for ferrimagnetisms, the partial replacement of Fe ion of bigger ionic radius by the Cr^{3+} ion of comparatively smaller ionic radius reduces the Fe^{3+} composition on the [B] site, which in rotate (A-B) super exchange reactions [47]. In other words, possible reason for the decrease in saturation magnetization is an increase in canting angles between magnetic moments on B lattice sites. An experimental value of the Bohr magneton number \(~({\eta _{\rm B}})\) was estimated using standard relation [48].

$${\eta _{\rm B}}=~\frac{{\left({{{\text{M}}_{\text{s}}}} \right) \times ({{\text{M}}_{\text{w}}})}}{{5585}}$$

(6)

where \({\eta _{\rm B}}\) is magneton number in \({\mu _B}\), M_w is the molecular weight in g and M_s is saturation magnetization in emu/g. The estimated Bohr magneton numbers with zinc and chromium concentration are presented in Table 5. The anisotropy constant (K) can be estimated using standrad relation and the values are tabulated in Table 6 [49].

Table 6 The anisotropy constant (K), and anisotropy field (H_k) for before and after gamma irradiation samples $Ni_{1-x}Zn_xFe_{2-x}Cr_xO_4$ nanoparticles

$$K=~\frac{{\left({{{\text{M}}_{\text{s}}}} \right) \times ({{\text{H}}_{\text{c}}})}}{{0.98}}$$

(7)

where K is the anisotropy constant, M_s is the saturation magnetization in emu/g and H_c is coercivity. The values of anisotropy constant (K) depends substituted ions and affected by spin canting. The decrease in anisotropy constant indicates the decrease in domain wall energy. The anisotropy field which binds the magnetization in a preferred direction is indirect measurements of the crystal anisotropy forces were determined using the following standard relation are listed in Table 6 [50].

$${{\text{H}}_{\text{K}}}=\frac{{2{{\text{K}}_1}}}{{{\text{M}}_{\text{s}}}}$$

(8)

where, H_K is the anisotropy field, K_1 is the anisotropy constant and M_S is the saturation magnetization.

3.5 Dielectric properties analysis

The behavior of dielectric properties study for spinel ferrites which clearly depends on various factors, including sintering temperature, chemical compositions, density, crystallite size and synthesizing method. The dielectric properties of unirradiated and after γ-irradiated of all the prepared samples were measured by the LCR-Q meter at room temperature (R.T.) with the frequency range of 50 Hz to 5 MHz. The dielectric constant (ε') and dielectric loss tangent (tan \(\delta\)) of all the samples were

calculated using standard relation (9–10) [51, 52].

$$\varepsilon ^{\prime}=\frac{{Cd}}{{{\varepsilon _0}A}}~$$

(9)

$$\tan ~\delta =\frac{{\varepsilon ^{\prime}}}{{\varepsilon ^{\prime\prime}}}$$

(10)

where, C = capacitance of the parallel plate capacitor, d = thickness of the pellets, \({\varepsilon _0}\) = dielectric permittivity of free space (\({\varepsilon _0}=~\)8.854 \(\times\) 10^{-14} F/cm) and A-cross-sectional area of the pellet. The frequency dependent on the dielectric constant for (ε') $Ni_{1-x}Zn_xFe_{2-x}Cr_xO_4$ nanoparticles are in very good agreement with the other ferrite [53]. The dielectric constant decrease with increase in applied frequency is shown in Fig. 8(a, b). The dielectric constant decreases with Zn–Cr ions substitution in Ni-ferrite and also decreased after γ-irradiation. Similar results were observed in the literature [39]. All the samples indicated dispersion due to Maxwell–Wagner interfacial (space charge) polarization is in agreement with Koop's Phenomenological theory [54, 55]. In ferrites, the dielectric polarization decreases with increase in frequency and also the conduction mechanism. The polarization is a strong correlation between the dielectric behavior and the conduction mechanism of ferrites. Based on the Electron hopping between $Fe^{3+} \leftrightarrow Fe^{2+} + e^-$ ions one gives the local displacement of the electrons in the direction of the applied field. The high value of dielectric constant at low frequency is due to the large number of species like Fe^{2+} ions, oxygen vacancies, interfacial dislocation piles up, grain boundary defects etc. It is excellent that the effect of the polarization is to decrease the field inside in the medium.

Fig. 8

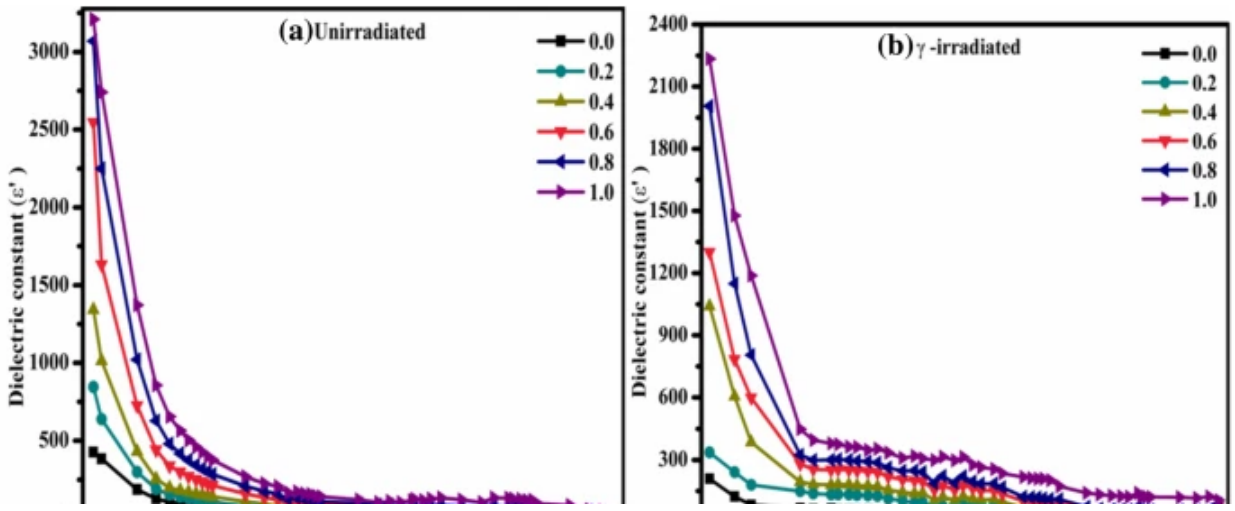

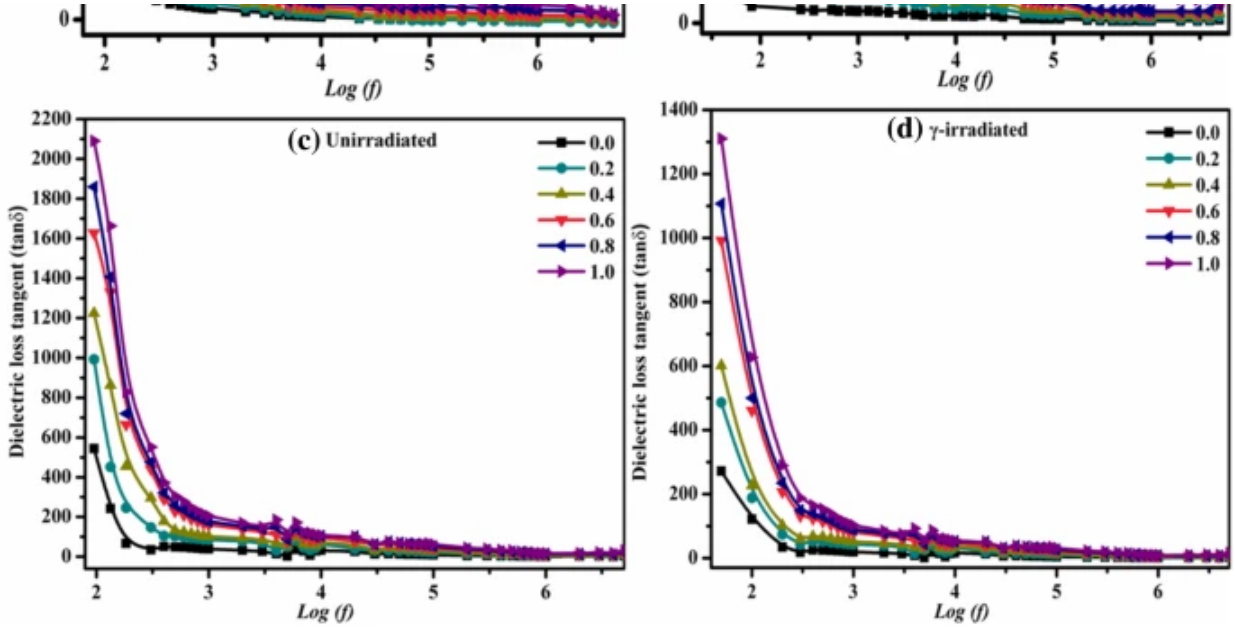

(**a, c**) Frequency dependence of dielectric constant. (**b, d**) Frequency dependence of dielectric loss tangent of unirradiated and \(~\gamma\)-irradiated for NPs $Ni_{1-x}Zn_xFe_{2-x}Cr_xO_4$ Nps

Figure 8(c, d) shows the variation of the dielectric loss tangent (tan \(\delta\)) with the frequency of unirradiated and irradiated of all the samples. All of the concentrations show normal variation and an exponential decrease in the dielectric loss tangent with increasing frequency. Therefore, low dielectric loss tangent is attractive potential applications in devices obtained for all the prepared samples. The high value of dielectric loss tangent (tan \(\delta\)) at low frequency corresponds to grain boundary further energy is essential for electron exchange between $Fe^{3+} \leftrightarrow Fe^{2+} + e^-$ ions. The maximum in the dielectric loss tangent occurs at relatively low frequency and decreases with increasing frequency. Finally, it can be observed that dielectric loss tangent (tan \(\delta\)) decreases with increase in zinc and chromium concentration and also after γ-irradiation.

4 Conclusion

Nickel ferrite nanoparticles simultaneously substituted zinc and chromium with general chemical formula $Ni_{1-x}Zn_xFe_{2-x}Cr_xO_4$ with (x = 0.0, 0.2, 0.4, 0.6, 0.8 and 1.0) have been successfully synthesized by employing sol–gel auto-combustion method. All the prepared samples have been gamma irradiated with ^{60}Co radioactive source. The effect of γ-irradiation with a dose of 7 Mrad on the some structural, morphological and magnetic properties has been investigated. X-ray diffractions and also FT-IR reveals the formation of single cubic spinel crystal structure. The lattice parameters 'a' decreases after γ-irradiation for corresponding compositions. The crystallite sizes (t) are reduced which calculated from

a most intense peak (311) and it is observed within the range of 19–28 nm and 18–22 nm for un-irradiated and after γ-irradiation respectively. FE-SEM investigates designate that after γ-irradiated causes amorphization, in particular at the grain boundaries. Grain size (G) of Ni–Zn–Cr ferrite nanoparticles were estimated from FE-SEM un-irradiated and after γ-irradiated and it can be found in the range of 38–50 nm. M-H loops recorded at room temperature exhibits a typical hysteresis indicating the ferrimagnetic nature of the samples. After γ-irradiation of Ni–Zn–Cr ferrite nanoparticles creates defects in the material which renders the physical properties manufacture it technological additional relevant.

References

1. W. Hu, N. Qin, G. Wu, Y. Lin, S. Li, D. Bao, Opportunity of spinel ferrite materials in nonvolatile memory device applications based on their resistive switching performances. J. Am. Chem. Soc. **134**, 14658–14661 (2012)

Article Google Scholar

2. M.-S. Cao, W.-L. Song, Z.-L. Hou, B. Wen, J. Yuan, The effects of temperature and frequency on the dielectric properties, electromagnetic interference shielding and microwave-absorption of short carbon fiber/silica composites. Carbon **48**, 788–796 (2010)

Article Google Scholar

3. M. Pardavi-Horvath, Microwave applications of soft ferrites. J. Magn. Magn. Mater. **215**, 171–183 (2000)

Article Google Scholar

4. A. Akbarzadeh, M. Samiei, S. Davaran, Magnetic nanoparticles: preparation, physical properties, and applications in biomedicine. Nanoscale Res. Lett. **7**, 144 (2012)

Article Google Scholar

5. A. Sattar, H. El-Sayed, I. ALsuqia, Structural and magnetic properties of $CoFe_2O_4$/$NiFe_2O_4$ core/shell nanocomposite prepared by the hydrothermal method. J. Magn. Magn. Mater. **395**, 89–96 (2015)

Article Google Scholar

6. S. Karimi, P. Kameli, H. Ahmadvand, H. Salamati, Effects of Zn–Cr-substitution on the structural and magnetic properties of $Ni_{1-x}Zn_xFe_{2-x}Cr_xO_4$ ferrites. Ceram. Int. **42**, 16948–16955 (2016)

Article Google Scholar

7. M.A. Gabal, Y. Al Angari, Effect of diamagnetic substitution on the structural, magnetic and electrical properties of $NiFe_2O_4$. Mater. Chem. Phys. **115**, 578–584 (2009)

Article Google Scholar

8. M. Gabal, R.M. El-Shishtawy, Y. Al Angari, Structural and magnetic properties of nano-crystalline Ni–Zn ferrites synthesized using egg-white precursor. J. Magn. Magn. Mater. **324**, 2258–2264 (2012)

Article Google Scholar

9. A. Ghasemi, M. Mousavinia, Structural and magnetic evaluation of substituted $NiZnFe_2O_4$ particles synthesized by conventional sol–gel method. Ceram. Int. **40**, 2825–2834 (2014)

Article Google Scholar

10. M. Amer, A. Tawfik, A. Mostafa, A. El-Shora, S. Zaki, Spectral studies of Co substituted Ni–Zn ferrites. J. Magn. Magn. Mater. **323**, 1445–1452 (2011)

Article Google Scholar

11. S. Muralidharan, V. Saraswathy, L.J. Berchmans, K. Thangavel, K.Y. Ann, Nickel ferrite ($NiFe_2O_4$): a possible candidate material as reference electrode for corrosion monitoring of steel in concrete environments. Sens. Actuators B **145**, 225–231 (2010)

Article Google Scholar

12. J. Gunjakar, A. More, K. Gurav, C. Lokhande, Chemical synthesis of spinel nickel ferrite ($NiFe_2O_4$)

nano-sheets. Appl. Surf. Sci. **254**, 5844–5848 (2008)

Article Google Scholar

13. A. Ziarati, A. Sobhani-Nasab, M. Rahimi-Nasrabadi, M.R. Ganjali, A. Badiei, Sonication method synergism with rare earth based nanocatalyst: preparation of $NiFe_{2-x}Eu_xO_4$ nanostructures and its catalytic applications for the synthesis of benzimidazoles, benzoxazoles, and benzothiazoles under ultrasonic irradiation. J. Rare Earth **35**, 374–381 (2017)

Article Google Scholar

14. M. Jalaly, M. Enayati, P. Kameli, F. Karimzadeh, Effect of composition on structural and magnetic properties of nanocrystalline ball milled $Ni_{1-x}Zn_xFe_2O_4$ ferrite. Phys. B **405**, 507–512 (2010)

Article Google Scholar

15. E. Pervaiz, I. Gul, High frequency AC response, DC resistivity and magnetic studies of holmium substituted Ni-ferrite: a novel electromagnetic material. J. Magn. Magn. Mater. **349**, 27–34 (2014)

Article Google Scholar

16. L.-Z. Li, X.-Q. Tu, R. Wang, L. Peng, Structural and magnetic properties of Cr-substituted NiZnCo ferrite nanopowders. J. Magn. Magn. Mater. **381**, 328–331 (2015)

Article Google Scholar

17. T.S. Saraf, J.S. Kounsalye, S.D. Birajdar, N. Shamkuwar, Nd: YAG laser irradiation effects on structural and magnetic properties of $Ni_{1+x}Zr_xFe_{2-2x}O_4$ nanoparticles. Radiat. Phys. Chem. **146**, 96–104 (2018)

Article Google Scholar

18. M. Rahimi-Nasrabadi, M. Behpour, A. Sobhani-Nasab, M.R. Jeddy, Nanocrystalline Ce-doped copper ferrite: synthesis, characterization, and its photocatalyst application. J. Mater. Sci.: Mater. Electron. **27**, 11691–11697 (2016)

Google Scholar

19. R.B. Borade, S.E. Shirsath, G. Vats, A.S. Gaikwad, S.M. Patange, S.B. Kadam, R.H. Kadam, A.B. Kadam, Polycrystalline to preferred-(100) single crystal texture phase transformation of yttrium iron garnet nanoparticles. Nanoscale Adv. (2018). https://doi.org/10.1039/C8NA00123E

Google Scholar

20. S. Joshi, M. Kumar, S. Chhoker, G. Srivastava, M. Jewariya, V. Singh, Structural, magnetic, dielectric and optical properties of nickel ferrite nanoparticles synthesized by co-precipitation method. J. Mol. Struct. **1076**, 55–62 (2014)

Article Google Scholar

21. S. Phumying, S. Labuayai, E. Swatsitang, V. Amornkitbamrung, S. Maensiri, Nanocrystalline spinel ferrite (MFe2O4, M=Ni, Co, Mn, Mg, Zn) powders prepared by a simple aloe vera plant-extracted solution hydrothermal route. Mater. Res. Bull. **48**, 2060–2065 (2013)

Article Google Scholar

22. A. Javidan, M. Ramezani, A. Sobhani-Nasab, S.M. Hosseinpour-Mashkani, Synthesis, characterization, and magnetic property of monoferrite $BaFe_2O_4$ nanoparticles with aid of a novel precursor. J. Mater. Sci.: Mater. Electron. **26**, 3813–3818 (2015)

Google Scholar

23. T. Marinca, I. Chicinaş, O. Isnard, V. Pop, F. Popa, Synthesis, structural and magnetic characterization of nanocrystalline nickel ferrite-$NiFe_2O_4$ obtained by reactive milling. J. Alloy. Compd. **509**, 7931–7936 (2011)

Article Google Scholar

24. N. Chaudhari, R. Kambale, D. Bhosale, S. Suryavanshi, S. Sawant, Thermal hysteresis and domain states in Ni–Zn ferrites synthesized by oxalate precursor method. J. Magn. Magn. Mater. **322**, 1999–2005 (2010)

Article Google Scholar

25. M.A. Dar, J. Shah, W. Siddiqui, R. Kotnala, Study of structure and magnetic properties of Ni–Zn ferrite nano-particles synthesized via co-precipitation and reverse micro-emulsion technique. Appl. Nanosci. **4**, 675–682 (2014)

Article Google Scholar

26. D.A. Dupree, T. Nguyen, D. Panescu, J.G. Whayne, D. McGee, D.K. Swanson, Interactive systems and methods for controlling the use of diagnostic or therapeutic instruments in interior body regions, in, Google Patents (2004)

27. D. Baker, S. Kanekal, V. Hoxie, S. Batiste, M. Bolton, X. Li, S. Elkington, S. Monk, R. Reukauf, S. Steg, The relativistic electron-proton telescope (rept) instrument on board the radiation belt storm probes (rbsp) spacecraft: characterization of earth's radiation belt high-energy particle populations, in *The Van Allen Probes Mission* (Springer, 2012), pp. 337–381

28. N. Okasha, S. El Dek, M. Abdelmaksoud, D.N. Ghaffar, Enhanced structure and magnetic properties of doped nanomagnetite by γ-irradiation. J. Alloy. Compd. **737**, 356–364 (2018)

Article Google Scholar

29. R. Lisha, T. Hysen, P. Geetha, P. Aravind, M. Shareef, A. Shamlath, S. Ojha, R. Ramanujan, M. Anantharaman, Defect induced enhancement of exchange bias by swift heavy ion irradiation in zinc ferrite–FeNiMoB alloy based bilayer films. Nucl. Instrum. Methods Phys. Res. Sect. B: Beam Interact. Mater. Atoms **360**, 68–74 (2015)

Article Google Scholar

30. T.-R. Kuo, V.A. Hovhannisyan, Y.-C. Chao, S.-L. Chao, S.-J. Chiang, S.-J. Lin, C.-Y. Dong, C.-C. Chen, Multiple release kinetics of targeted drug from gold nanorod embedded polyelectrolyte conjugates induced by near-infrared laser irradiation. J. Am. Chem. Soc. **132**, 14163–14171 (2010)

Article Google Scholar

31. I. Hamada, X-ray diffraction and IR absorption in the system $Co_{0.6}Zn_{0.4}Mn_xFe_{2-x}O_4$ before and after γ-irradiation. J. Magn. Magn. Mater. **271**, 318–325 (2004)

Article Google Scholar

32. M.L. Mane, R. Sundar, K. Ranganathan, S. Oak, K. Jadhav, Effects of Nd: YAG laser irradiation on structural and magnetic properties of $Li_{0.5}Fe_{2.5}O_4$. Nucl. Instrum. Methods Phys. Res. Sect. B: Beam Interact. Mater. Atoms **269**, 466–471 (2011)

Article Google Scholar

33. V.J. Angadi, A. Anupama, R. Kumar, H. Somashekarappa, S. Matteppanavar, B. Rudraswamy, B. Sahoo, Dose dependent modifications in structural and magnetic properties of γ-irradiated nanocrystalline $Mn_{0.5}Zn_{0.5}Fe_2O_4$ ceramics. Ceram. Int. **43**, 523–526 (2017)

Article Google Scholar

34. A. Karim, S.E. Shirsath, S. Shukla, K. Jadhav, Gamma irradiation induced damage creation on the cation distribution, structural and magnetic properties in Ni–Zn ferrite. Nucl. Instrum. Methods Phys. Res. Sect. B: Beam Interact. Mater. Atoms **268** 2706–2711 (2010)

Article Google Scholar

35. D. Carta, M.F. Casula, A. Falqui, D. Loche, G. Mountjoy, C. Sangregorio, A. Corrias, A structural and magnetic investigation of the inversion degree in ferrite nanocrystals MFe2O4 (M=Mn, Co, Ni). J. Phys. Chem. C **113**, 8606–8615 (2009)

Article Google Scholar

36. V.K. Mande, D.N. Bhoyar, S. Vyawahare, K. Jadhav, Effect of Zn^{2+}–Cr^{3+} substitution on structural, morphological, magnetic and electrical properties of $NiFe_2O_4$ ferrite nanoparticles. J. Mater. Sci.: Mater. Electron. **29**, 15259–15270 (2018)

Google Scholar

37. A. Hussain, T. Abbas, S.B. Niazi, Preparation of $Ni_{1-x}Mn_xFe_2O_4$ ferrites by sol–gel method and

study of their cation distribution. Ceram. Int. **39**, 1221–1225 (2013)

Article Google Scholar

38. M. Kooti, A.N. Sedeh, Synthesis and characterization of $NiFe_2O_4$ magnetic nanoparticles by combustion method. J. Mater. Sci. Technol. **29**, 34–38 (2013)

Article Google Scholar

39. M. Veena, A. Somashekarappa, G. Shankaramurthy, H. Jayanna, H. Somashekarappa, Effect of ^{60}Co gamma irradiation on dielectric and complex impedance properties of Dy^{3+} substituted Ni–Zn nanoferrites. J. Magn. Magn. Mater. **419**, 375–385 (2016)

Article Google Scholar

40. A. Birajdar, S.E. Shirsath, R. Kadam, S. Patange, D. Mane, A. Shitre, Frequency and temperature dependent electrical properties of $Ni_{0.7}Zn_{0.3}Cr_xFe_{2-x}O_4$ ($0 \le x \le 0.5$). Ceram. Int. **38**, 2963–2970 (2012)

Article Google Scholar

41. J.S. Kounsalye, P.B. Kharat, M.V. Shisode, K. Jadhav, Influence of Ti^{4+} ion substitution on structural, electrical and dielectric properties of $Li_{0.5}Fe_{2.5}O_4$ nanoparticles. J. Mater. Sci.: Mater. Electron. **28**, 17254–17261 (2017)

Google Scholar

42. M. Mantina, A.C. Chamberlin, R. Valero, C.J. Cramer, D.G. Truhlar, Consistent van der Waals radii for the whole main group. J. Phys. Chem. A **113**, 5806–5812 (2009)

Article Google Scholar

43. M. Khairy, Synthesis, characterization, magnetic and electrical properties of polyaniline/$NiFe_2O_4$ nanocomposite. Synth. Met. **189**, 34–41 (2014)

Article Google Scholar

44. M. Rahimi-Nasrabadi, M. Behpour, A. Sobhani-Nasab, S.M. Hosseinpour-Mashkani, $ZnFe_{2-x}La_xO_4$ nanostructure: synthesis, characterization, and its magnetic properties. J. Mater. Sci.: Mater. Electron. **26**, 9776–9781 (2015)

Google Scholar

45. A. Sobhani-Nasab, Z. Zahraei, M. Akbari, M. Maddahfar, S.M. Hosseinpour-Mashkani, Synthesis, characterization, and antibacterial activities of $ZnLaFe_2O_4/NiTiO_3$ nanocomposite. J. Mol. Struct. **1139**, 430–435 (2017)

Article Google Scholar

46. M. George, A.M. John, S.S. Nair, P. Joy, M. Anantharaman, Finite size effects on the structural and magnetic properties of sol–gel synthesized $NiFe_2O_4$ powders. J. Magn. Magn. Mater. **302**, 190–195 (2006)

Article Google Scholar

47. P. Hankare, U. Sankpal, R. Patil, I. Mulla, R. Sasikala, A. Tripathi, K. Garadkar, Synthesis and characterization of nanocrystalline zinc substituted nickel ferrites. J. Alloy. Compd. **496**, 256–260 (2010)

Article Google Scholar

48. G. Balasubramanian, P. Neumann, D. Twitchen, M. Markham, R. Kolesov, N. Mizuochi, J. Isoya, J. Achard, J. Beck, J. Tissler, Ultralong spin coherence time in isotopically engineered diamond. Nat. Mater. **8**, 383 (2009)

Article Google Scholar

49. K.C.B. Naidu, W. Madhuri, Microwave processed NiMg ferrite: studies on structural and magnetic

properties. J. Magn. Magn. Mater. **420**, 109–116 (2016)

Article Google Scholar

50. R. Kambale, K. Song, Y. Koo, N. Hur, Low temperature synthesis of nanocrystalline Dy^{3+} doped cobalt ferrite: structural and magnetic properties. J. Appl. Phys. **110**, 053910 (2011)

Article Google Scholar

51. V. Sunny, P. Kurian, P. Mohanan, P. Joy, M. Anantharaman, A flexible microwave absorber based on nickel ferrite nanocomposite. J. Alloy. Compd. **489**, 297–303 (2010)

Article Google Scholar

52. M. Mallapur, P. Shaikh, R. Kambale, H. Jamadar, P. Mahamuni, B. Chougule, Structural and electrical properties of nanocrystalline cobalt substituted nickel zinc ferrite. J. Alloy. Compd. **479**, 797–802 (2009)

Article Google Scholar

53. N. Chandamma, S. Kumar, G. Shankarmurthy, E. Melagiriyappa, K. Nagaraja, Effect of gamma irradiation on some electrical and dielectric properties of Ce^{3+} substituted Ni–Zn nano ferrites. Chin. J. Phys. **55**, 1729–1738 (2017)

Article Google Scholar

54. F. Rogti, M. Ferhat, Maxwell–Wagner polarization and interfacial charge at the multi-layers of thermoplastic polymers. J. Electrostat. **72**, 91–97 (2014)

Article Google Scholar

55. R. Ali, A. Mahmood, M.A. Khan, A.H. Chughtai, M. Shahid, I. Shakir, M.F. Warsi, Impacts of Ni–Co substitution on the structural, magnetic and dielectric properties of magnesium nano-ferrites fabricated by micro-emulsion method. J. Alloy. Compd. **584**, 363–368 (2014)

Article Google Scholar

Acknowledgements

The author VKM would like to thank, The Government Institute of Science, Aurangabad, (M.H.) India, for providing gamma radiation facility.

Author information

Authors and Affiliations

Department of Physics, Dr. Babasaheb Ambedkar Marathwada University, Aurangabad, MS, India
Vishwanath K. Mande, Jitendra S. Kounsalye & K. M. Jadhav

Department of Physics and Research Center, Deogiri College, Aurangabad, MS, India
S. K. Vyawahare

Corresponding author

Correspondence to K. M. Jadhav.

Rights and permissions

About this article

Cite this article

Mande, V.K., Kounsalye, J.S., Vyawahare, S.K. *et al.* Effect of γ-radiation on structural, morphological, magnetic and dielectric properties of Zn–Cr substituted nickel ferrite nanoparticles. *J Mater Sci: Mater Electron* **30**, 56–68 (2019). https://doi.org/10.1007/s10854-018-0252-1

Received
31 August 2018

Accepted
17 October 2018

Published
01 November 2018

Issue Date
15 January 2019

DOI
https://doi.org/10.1007/s10854-018-0252-1

Share this article

Anyone you share the following link with will be able to read this content:

Get shareable link

Provided by the Springer Nature SharedIt content-sharing initiative